



Application of Response Surface Methodology to Modeling and Optimization of Removal of Bismarck Brown and Thymol Blue by Mn-Fe₂O₄- NPs-AC: (Kinetics and Thermodynamic Studies)

SAIDEH BAGHERI*

Department of Chemistry, Science and Research Branch,
Islamic Azad University, Tehran P.O.Box14515-755, Tehran ,Iran.
Corresponding author E-mail: s_bagheri2010@yahoo.com

<http://dx.doi.org/10.13005/ojc/320163>

(Received: January 01, 2016; Accepted: March 04, 2016)

ABSTRACT

The focus of this research is on the rapid ultrasound-assisted removal of Bismarck Brown (BB) and Thymol Blue (TB) dyes from aqueous solutions using Mn-Fe₂O₄ nanoparticles loaded on activated carbon (Mn-Fe₂O₄- NPs-AC) as a low cost and environmental friendly adsorbent. The adsorbent was characterized by SEM, FTIR and XRD. The effect of variables such as initial concentration of BB, initial concentration of TB, pH of the solution, adsorbent dosage and sonication time on the removal percentages of BB and TB dyes were simultaneously investigated by central composite design (CCD) under response surface methodology (RSM). It was shown that the adsorption of BB and TB follows the pseudo-second-order rate equation, while the Langmuir model explains equilibrium data. Isotherms had also been used to obtain the thermodynamic parameters such as free energy (ΔG°), enthalpy (ΔH°) and entropy (ΔS°) of adsorption. The negative value of ΔG° indicates the feasibility and spontaneity of the adsorption process. The positive ΔH° suggests the endothermic nature of the adsorption. The positive values of ΔS° reflect the affinity of Mn-Fe₂O₄- NPs-AC towards BB and TB dyes. A small amount of the adsorbent was able to remove more than 99.0% of both dyes rapidly with high adsorption capacity in binary-component system (70.3 mg/g for BB, and 48.48 mg/g for TB).

Key words: Nanoparticle-loaded activated carbon, Response surface methodology, Ultrasound-assisted dye removal, Thymol Blue, Bismarck Brown.

INTRODUCTION

The industrial waste water such as textile waste water contains plenty of toxic dyes which are harmful for ecosystems and humans^{1,2}. Among the

several types of dyes including anionic (reactive dyes), cationic (basic dyes), and non-anionic (disperse dyes), the cationic ones are the most toxic dyes³. Among several methods for dyes removal from aqueous solution such as membrane separation^{4,5}

chemical oxidation and adsorption, the adsorption technique is known as one of the efficient methods for dye removal⁶⁻⁸.

Bismarck Brown (BB) as a basic dye is used in textile and leather biological stain. The solution of this odorless powder in water is brown⁹. Thymol Blue (TB), belonging to triphenylmethane group, has biological activity like stain agent. The TB dye is also used as pH indicator in analytical chemistry. Inhalation lead to respiratory tract exposure and subsequently Symptoms include coughing and shortness of breath. Skin Contact might cause irritation with redness and pain¹⁰.

Metal oxide nanoparticles, with their potential applications in the fields of physics, chemistry, biology, and medicine has attracted increasing research attention from the past decades because of their interesting physical and chemical properties. Over the last decade, magnetic nanoparticles (MNPs) are of great interest for researchers from a wide range of disciplines, including magnetic fluids¹¹, catalysis^{12, 13} biotechnology/biomedicine¹⁴, magnetic resonance imaging^{15, 16}, data storage¹⁷ and environmental remediation^{18, 19}. Super paramagnetic iron oxide nanoparticles have received increasing attention in areas as different as physics, chemistry, materials science, biology, and medicine, motivated by their unusual surface and magnetic properties²⁰.

Conventional and classical optimization protocol (one at a time) failed to give useful knowledge about the interaction between variables while requiring intensive labor and consuming long time because of requiring high number of experiments. Central composite design (CCD) under response surface methodology (RSM) can efficiently be applied for handling both variables involved and responses without suffering above-mentioned drawbacks. This approach enables researchers to make a suitable predictive model to apply for several factors even in the presence of complex interactions to describe responses and find the optimal conditions with less time elapsed²¹⁻²².

In the present work, Mn-Fe₂O₄ nanoparticle-loaded on AC(Mn-Fe₂O₄ -NPs-AC) as a novel adsorbent was simply synthesized and subsequently characterized by scanning electron microscopy(SEM),

Fourier transform infrared spectroscopy(FTIR) and X-ray diffraction(XRD) analysis. The influence of important variables (BB concentration, TB concentration, pH, amount of adsorbent and sonication time) were investigated and optimized by central composite design (CCD) under response surface methodology (RSM). It was shown that the adsorption of BB and TB follows the pseudo-second-order rate equation. The Langmuir model was found to be applied for the equilibrium data explanation. The EXPERT, a statistical software package was used for experimental design analysis and their subsequent regression analysis.

MATERIALS AND METHODS

Materials and instruments

Bismarck Brown 4,4'-[1,3-Phenylenebis(azo)]-bis[1,3-phenyldiamin] and Thymol Blue 3,3-bis(4-hydroxy-5-isopropyl-2-methylphenyl)-3H- benzo[c][1,2] oxathiole 1,1-dioxide are fully described in Table1. They were supplied from Merck(Darmstadt, Germany). The stock solution (100mg/L) of each dye was achieved following dissolution of 10 mg of which in 100 mL double distilled water, separately and suitable dilute on was performed to obtain working solution with desired concentration. The Mn-Fe₂O₄-NPs-AC was prepared and characterized by XRD and SEM. The morphology of the Mn-Fe₂O₄ -NPs-AC was observed by scanning electron microscopy (SEM; HitachiS-4160). X-ray diffraction (XRD) pattern was recorded by an automated Philips X'PertX-ray diffractometer with CuK α radiation (40 kV and 30 mA) for 2 θ values over 10–80°. Fourier transform infrared spectroscopy (FTIR in the range of 500–4000 cm⁻¹) of the adsorbent was recorded using FTIR spectrophotometer (Model:FT-IR JASCO 460 Plus). The spectra obtained were analyzed. The PH measurements were carried out using pH/Ion meter model-728 (Metrohm, Switzerland, Swiss) and the BB and TB concentrations were determined using Jasco UV-Vis spectrophotometer model V-530 (Jasco, Japan) at wave-lengths of 448 nm and 650 nm, respectively.

An ultrasonic bath with heating system (Tecno-GAZ SPA Ultra Sonic System, Korea) at frequency 50 Hz and power 296W was used for the ultrasound-assisted adsorption procedure. The STATISTICA, a statistical software package version

10.0 (Stat Soft Inc., Tulsa, USA), was used for experimental design analysis and their subsequent regression analysis.

Ultrasound-assisted multi-component adsorption of BB and TB on to Mn-Fe₂O₄-NPs-AC

A batch process using Mn-Fe₂O₄-NPs-AC in presence of ultrasound was applied for binary adsorption of BB and TB, while all experiments were under taken in a cylindrical glass vessel by adding 0.03g of adsorbent to 50 ml of BB and TB at PH 6.0 as optimum value. The vessel was immersed in an ultrasonic bath for 5 min at room temperature and subsequently the solutions were centrifuged. Then, non-adsorbed dye contents were determined by using UV-Vis spectrophotometer set at wavelengths 448 and 650 nm for BB and TB, respectively.

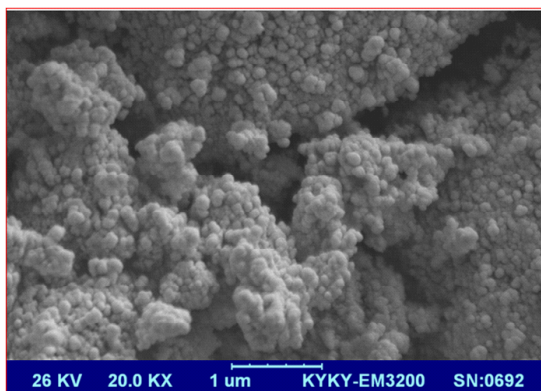


Fig. 1: The SEM image of the prepared Mn-Fe₂O₄- NPs-AC

Measurements of dye uptake

The dye concentrations were determined from calibration curve obtained at maximum wavelength over working concentration range. The efficiency of dyes removal was determined at different experimental conditions optimized using the CCD method. The experiments were also performed in the initial dye concentration range of 2-18 mg/L to obtain adsorption isotherms. The removal percentage of each dye was calculated using the following equation:

$$\% \text{ dye removal} = \frac{(C_0 - C_t)}{C_0} \times 100 \quad \dots(1)$$

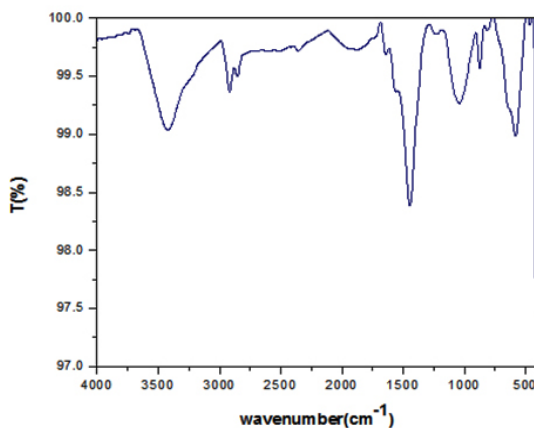


Fig. 2: FT-IR transmittance spectrum of the prepared Mn-Fe₂O₄- NPs-AC

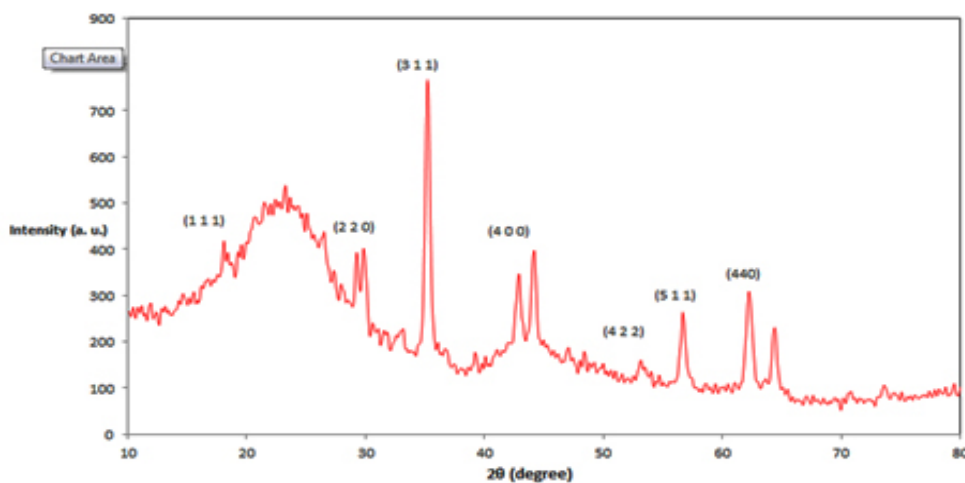


Fig. 3: XRD pattern of the prepared Mn-Fe₂O₄- NPs-AC

Where C_0 ($mg L^{-1}$) and C_t ($mg L^{-1}$) is the concentration of target at initial and after time t respectively.

$$q_t = \frac{(C_0 - C_t)V}{W} \quad \dots(2)$$

where C_0 ($mg L^{-1}$) and C_t ($mg L^{-1}$) are the initial dye concentration and equilibrium dye concentration in aqueous solution, respectively, V (L) is the solution volume and W (g) is the adsorbent mass.

Preparation of Mn-Fe₂O₄- NPs-AC

Activated carbon was purchased from Chem lab Company and used as a support material for the prepared MnFe₂O₄-NPs. The reaction solution for loading MnFe₂O₄ nanoparticles on activated carbon (Ac) was prepared as follows: The MnFe₂O₄ nano powders were synthesized by the conventional

co-precipitation method. The Fe (Cl)₃.6H₂O and Mn(Cl)₂. 4H₂O salts (molar ratio of Fe: Mn = 2:1) were dissolved in 300 mL pure water. Temperature of solution adjusted to 80^oC. Then while stirring and under nitrogen gas atmosphere, 50 mL of NaOH (2 M) were gently added to the solutions to adjust its pH; the solution was stirred for 2 h at 80 ^oC under N₂. Following this, the color of the bulk solution changed from orange to black. The black MnFe₂O₄ NPs were separated by an external permanent magnet. The precipitates were washed several times with deionized water and ethanol. The synthesized MnFe₂O₄ nanoparticles were dried in 70 ^oC for 12h and calcined at 500 ^oC for 4h in air, the nano-MnFe₂O₄ powders were obtained. Then in order to loaded MnFe₂O₄ nanoparticles on carbon active, 2g carbon active was added 200 ml ethanol and sonicated for 1 h. 0.4g MnFe₂O₄ nanoparticles was add to mixture, while mixture was sonicated .subsequence, prepared mixture was stirred for 20h. The obtained products were filtrated, washed

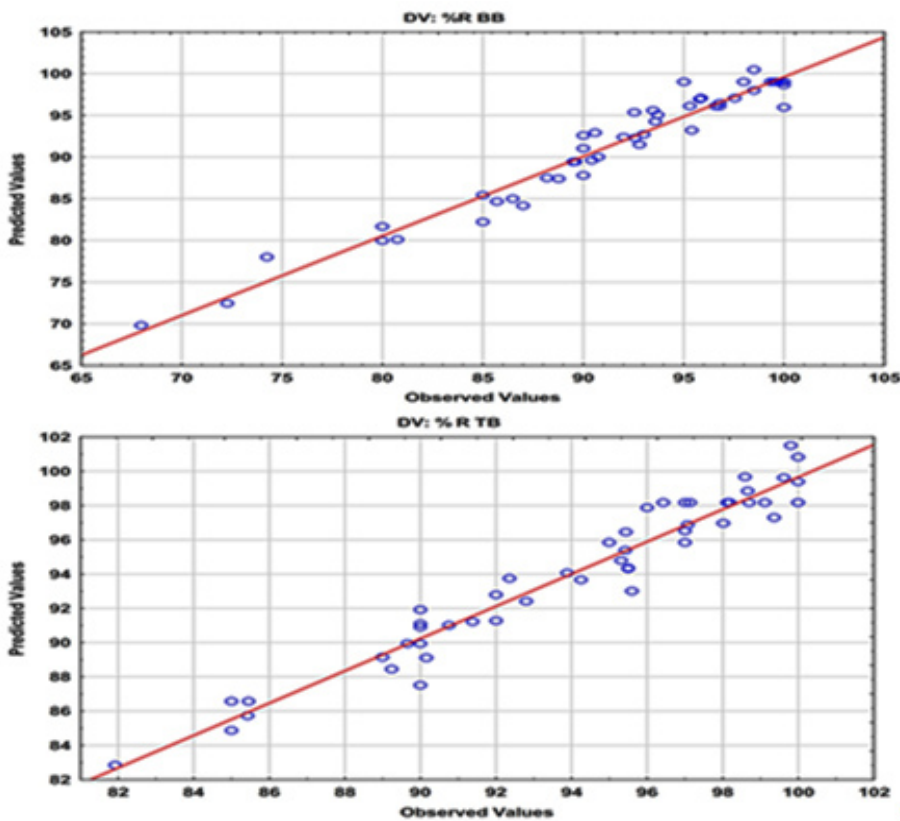


Fig. 4: (a) and (b) The experimental data versus predicted data for removal of BB and TB

and collected, then dried in a hot air oven at in 70 p C for 16 h. Finally the dried precipitate was grinded into powder form.

Central composite design

Response Surface Methodology is a statistical method that uses experimental data obtained from specified experimental design to model and optimize any process in which response of interest is influenced by several variables [23, 24]. Primarily, this optimization is done by following three major steps, viz., performing the statistically designed experiments, estimating the coefficients in a mathematical model, and predicting there sponses followed by examining the adequacy of the model[25]. RSM helps to enumerate the relationships between output variables called responses(y) and input variables called factors (X_i)²⁶.

$$y = f (X_1, X_2, X_3, \dots, X_n) \quad \dots(3)$$

CCD under RSM is suitable for fitting a quadratic surface to optimize the effective parameters and to investigate the contribution of variables and the interaction with minimum number of experiments²³. Generally, the CCD consists of 2^n factorial runs with $2n$ axial runs and n_c central runs where n is the number of variables($n=5$ in this work)²⁴, while the replication of central point gives a sense on numerical values of experimental errors and the data reproducibility. Thus, conducting 50 experiments permits the researchers for full study of all regions. Each experimental run was analyzed and the response was correlated with five input factors by using the following quadratic polynomial equation:

$$y = \beta_0 + \sum_{i=1}^5 \beta_i X_i + \sum_{i=1}^5 \sum_{j=1}^5 \beta_{ij} X_i X_j + \sum_{i=1}^5 \beta_{ii} X_i^2 + \varepsilon \quad \dots(4)$$

where y is the predicted response (removal percentage); X_i 's are the independent variables (BB concentration, TB concentration, pH, amount of adsorbent and sonication time) that are known for each experimental run. The parameter β_0 is the model constant β_i is the linear coefficient; β_{ii} are the quadratic coefficients and β_{ij} are the cross-product coefficients and ε is the residual term. The regression analysis is used to fit the equations for

both responses to the experimental data and to estimate the statistical significance of the equation using the Statistical software.

Obtain an optimal response. The first or second-order polynomial equations obtained according to the experimental responses as well as their subsequent fitting and the analysis of variance (ANOVA) help to estimate the main contribution of variables involved and their interaction. The plot of three-dimensional graph leads to the generation of surface response applied for the prediction of best operating conditions according to P -values and F -values. In this work, the dependence of dyes removal percentages as responses on five factors such as the initial BB concentration, initial TB concentration, pH effect, amount of adsorbent and sonication time at five levels (Table2) was analyzed using the STATISTICA 10.0 according to 50 runs. Table 2 shows the experimental design points with variables coded values used in matrix of experiments("2,"1,0,+1,+2) consisting factorial points with $2n$ axial points and central points.

Desirability function (DF)

Desirability function (DF) creates a function for each individual response (y) leading to final output of global function (D), maximum value of which supports the achievement of optimum value[27]. The principle and application of desirability function for the best predication of real behavior of adsorption system was pointed out previously²⁸. The desirability profiles indicate the predicted levels of variables, which produce the most desirable responses.

RESULTS AND DISCUSSION

Characterization of adsorbent

The particle size and morphology of Mn-Fe₂O₄-NPs-AC were evaluated by SEM. Figure 1 shows that the synthesized particles are spherical with the radius of about 75 nm. Figure 2 shows the FT-IR spectrum of the prepared Mn-Fe₂O₄-NPs-AC which was recorded within 500–3500. The broad band at 3422 is related to the –OH group. The band at about 2917 could be assigned to the symmetrical stretching C–H group. The shoulder at wave number around 1640 may be due to the C=O stretching. The peak at 1444 and 1231 are corresponding to the asymmetric C–H group and the bands at low

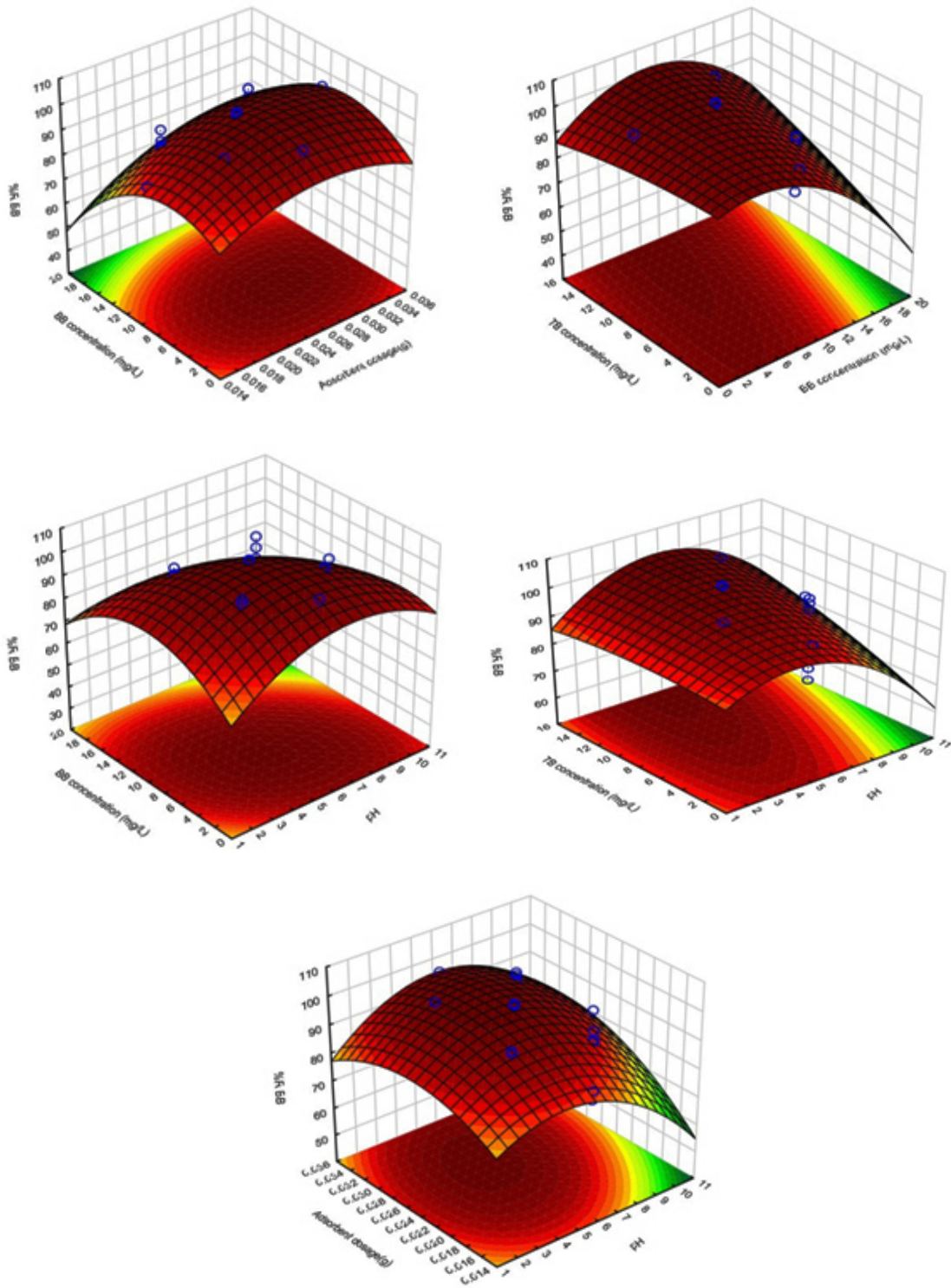


Fig. 5: Response surfaces for the dyes removal: (a) initial BB concentration–adsorbent dosage (b) initial TB concentration– initial BB concentration; (c) initial BB concentration– pH, (d) initial TB concentration– pH, (e) pH- adsorbent dosage

wave numbers ($d \approx 900$) are related to vibrations of the Fe–O and Mn–O bonds in manganese ferrite. These functional groups may act as anchoring sites for dye molecules as reported in the literature²⁹. The X-ray diffraction (XRD) pattern of Mn-Fe₂O₄–NPs-AC nanoparticles is shown in Figure 3. Seven characteristic peaks for Mn-Fe₂O₄–NPs-AC ($2\theta = 18.25^\circ, 29.27^\circ, 35.0^\circ, 44.15^\circ, 53.2^\circ, 56.69^\circ$ and 62.26°) corresponding to indices (111), (220), (311), (400), (422), (511) and (440), respectively. These patterns confirm the formation of cubic spinel type lattice of Mn-Fe₂O₄–NPs-AC nanoparticles. The

observed strong XRD peaks (Fig.3), indicate the well-crystallized structure of the prepared Mn-Fe₂O₄–NPs-AC while no characteristic peaks correspond to impurities such as Fe, Fe(OH)₂ and Fe(OH)₃ and/or other compounds, were detected.

Analysis of central composite design

As it is seen from CCD (Table 2), the effects of five dependent variables BB concentration (A), TB concentration (B), PH (C), amount of adsorbent (D) and time of sonication (E) were investigated. 50 experiments and their corresponding responses are

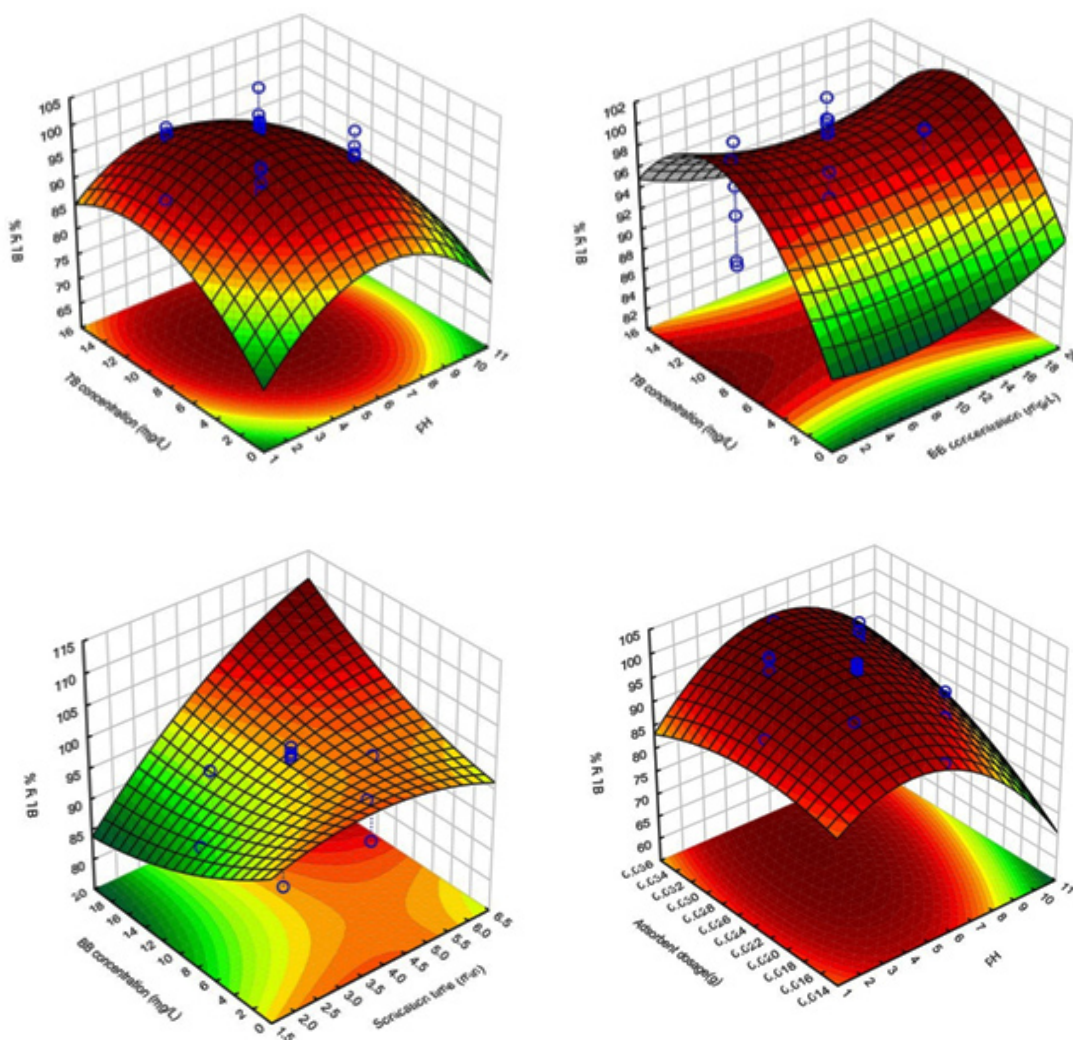


Fig. 6: Response surfaces for the dyes removal: (a) initial TB concentration– pH (b) initial TB concentration– initial BB concentration; (c) initial BB concentration– sonication time, (e) pH– adsorbent dosage

presented in Table 2. Analysis of variance (ANOVA) was performed for the removal percentage of each dye by using STATISTICA 10.0 (Table 2). The quality of the polynomial model equation was judged statistically by the coefficient of determination and its statistical significance was determined by *F*-test. *P*-values less than 0.05 are generally considered as a criterion for distinguishing statistically significant variables. However, Bonferroni test was applied to reduce alpha value to 0.01 which results in reducing the number of significant variables. As mentioned above, a *P*-value less than 0.01 (Bonferroni adjusted) indicates the statistical significance of each factor at 95% confidence level. Thus, the following predictive models describing the removal percentages of BB and TB dyes were obtained in terms of significant variables which satisfy the Bonferroni limit.

$$Y_{BB} = 99.018 - 6.7290A + 3.2493B - 4.2080C + 5.3355D + 3.8140E + 4.5872AB - 5.1675AC$$

$$+ 2.5679AD + 3.6788BC + 4.7161CD - 6.7661 - 10.649 - 8.2536 - 4.1486 \dots(5)$$

$$Y_{TB} = 98.176 - 1.5522B - 3.5335C + 3.9691D + 4.9135E + 2.6765AC + 3.4303AE - 2.2660BC + 4.3253CD - 5.1452 - 8.9166 - 3.2966 - 2.2516 \dots(6)$$

The plot of experimental *R*% values versus predicted ones indicated a good fit for both BB and TB (Fig.4). From ANOVA for the *R*%_{BB} and *R*%_{TB}, the *P*-values for the lack of fits corresponding to BB and TB were obtained to be 0.11 and 0.30, respectively which prove the applicability of the predictive models. For both models, the and adjusted were close to 1 confirming the goodness of the fit. From Eq. (5), it is seen that the pH and its interaction with both BB and TB concentrations are significant which negatively affect *R*%_{BB}. Another significant variable that positively affects *R*%_{BB} is amount of adsorbent. The trend in Eq. (6) corresponding to *R*%_{TB} is fairly

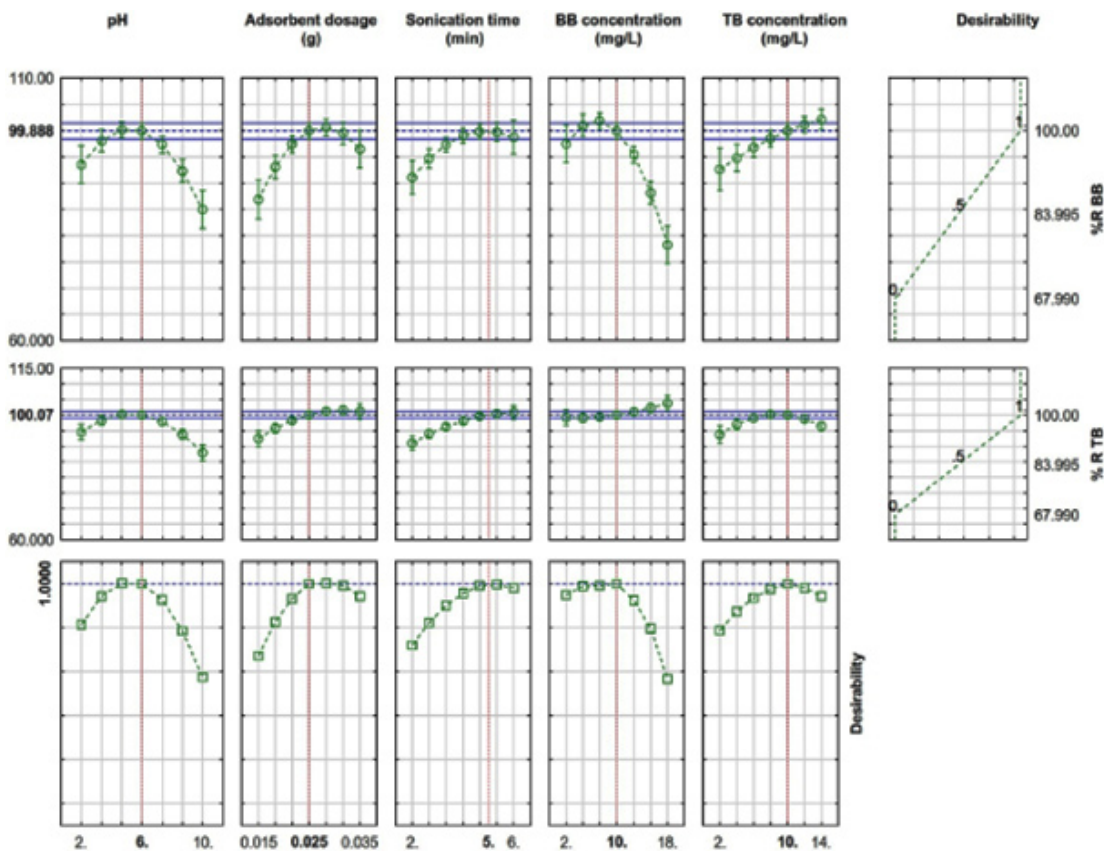


Fig.7: Profiles for predicted values and desirability function for removal percentage of BB and TB. Dashed line indicates current values after optimization

Table 1: Properties of the dyes

Properties	Bismarck Brown(BB)	Thymol Blue(TB)
Appearance	dark brown powder	Brownish-green powder
CAS number	10114-58-6	76-61-9
Chemical formula	C ₁₈ H ₁₆ N ₈ , 2HCL	C ₂₇ H ₃₀ O ₃₀ O ₅
Molecular weight (g/mol)	419.31	466.59
Maximum wavelength(λ_{max}) (nm)	448	650
Class	azo	Triphenyl methane
Use	textile, leather, biological stain	indicator, , biological stain

Runs	Block	A	B	C	D	E	BB removal (%)	TB removal (%)
1	1	14	6	4	0.03	5	89.6	100
2	1	6	14	8	0.02	3	89.49	85
3	1	6	6	8	0.03	3	93.6	90
4	1	6	14	8	0.02	5	92.54	85.45
5	1	14	6	4	0.02	5	86.5	97
6	1	14	14	8	0.02	5	85.71	90.15
7	1	14	14	4	0.02	5	92.58	95.5
8	1	14	14	8	0.02	3	80	81.92
9	1	10	10	6	0.035	4	96.79	98.66
10	1	6	6	8	0.02	5	95.87	95
11	1	10	10	2	0.025	4	90	92
12	1	10	10	6	0.015	4	85	90
13	1	14	6	8	0.02	5	72.26	95.5
14	1	14	6	4	0.03	3	90	92
15	1	10	10	6	0.025	4	99.65	97
16	1	14	14	4	0.02	3	88.18	89.24
17	1	14	6	4	0.02	3	85	89
18	1	6	14	8	0.03	5	93.48	90
19	1	14	6	8	0.03	5	80	99.8
20	1	14	14	4	0.03	3	92	91.38
21	1	6	14	8	0.03	3	98.5	92.8
22	1	14	14	4	0.03	5	95.31	96
23	1	10	10	6	0.025	4	99.8	98.7
24	1	14	6	8	0.03	3	80.73	95.6
25	1	6	6	8	0.03	5	97.56	97
26	1	10	10	10	0.025	4	87	85.42
27	1	10	18	6	0.025	4	95	100
28	1	10	10	6	0.025	4	99.5	98.18
29	1	6	6	4	0.03	3	93.7	92.35
30	1	6	6	8	0.02	3	88.78	90
31	1	14	14	8	0.03	3	90.42	89.65
32	1	2	10	6	0.025	4	100	99.62
33	1	10	12	6	0.025	2	90	90.75
34	1	14	6	8	0.02	3	67.99	85
35	1	6	14	4	0.02	3	90.75	93.89
36	1	6	14	4	0.02	5	96.6	95.43

37	1	6	6	4	0.02	5	95.81	95.44
38	1	10	10	6	0.025	4	98	96.43
39	1	10	10	6	0.025	4	100	99.12
40	1	6	6	4	0.03	5	98.51	99.36
41	1	18	10	6	0.025	4	74.24	98.59
42	1	10	10	6	0.025	4	100	98.11
43	1	6	14	4	0.03	3	92.8	95.31
44	1	10	10	6	0.025	6	100	100
45	1	6	6	4	0.02	3	90.6	94.25
46	1	6	14	4	0.03	5	96.8	97.08
47	1	10	10	6	0.025	4	99.35	97.14
48	1	14	14	8	0.03	5	95.42	98.02
49	1	10	2	6	0.025	4	93	90
50	1	10	10	6	0.025	4	99.6	100

Table 2: Experimental factors and levels in the central composite design

Factors	levels			Star point $\alpha = 2.37$	
	Low (-1)	Central (0)	High (+1)	$-\alpha$	$+\alpha$
Concentration (mg/L) (A)	6	10	14	2	18
Concentration (mg/L) (B)	6	10	14	2	18
pH (C)	2	6	10	2	10
adsorbent (g) (D)	0.02	0.025	0.030	0.015	0.035
Time (min) (E)	3	4	5	2	6

similar to that of BB. However, TB concentration significantly affects the $R\%_{TB}$ negatively in linear and quadratic ways. Furthermore, the interaction of the pH with amount of adsorbent played significant role in $R\%_{BB}$ and $R\%_{TB}$.

Response surface plots

The 3D RSM surfaces corresponding to $R\%_{BB}$ and $R\%_{TB}$ were depicted and considered to optimize the significant factors and to give useful information about the possible interaction of variables. As also seen from Eqs.(5) and (6), the effects of significant interaction terms on the curvature of the surfaces are observed as expected (Fig.5 and Fig.6). The maximum adsorption of BB and TB in high sonication time confirms high contribution of ultrasound in mass transfer supporting its requirement for obtaining maximum removal percentage. As seen from the results, the initial adsorption rate of adsorbent is accelerated due to high available surface area and vacant sites.

The RSM plots (Fig. 5a–c and Fig.6 a-c) presents the interaction of pH with initial BB concentration, initial TB concentration and adsorbent dosage respectively. The pH has negative correlation with removal percentage and at higher pH led to achievement of lower removal percentage. At low initial pH, protonation of the adsorbent functional groups led to generation of positive charge and appearance of the strong attractive forces between the cationic dye molecule and adsorbent surface (increase in removal percentage). (Fig. 5d) show the interaction of adsorbent dosage with initial dye concentration and their relation with removal percentage. It was seen that the removal percentage of each dye decreases at higher initial dye concentration. (Fig.5e) that the removal percentage changes *versus* the adsorbent dosage. The positive increase in the dye removal percentage with increase in adsorbent mass is seen. Significant diminish in removal percentage at lower amount of Mn-Fe₂O₄-NPs-AC is attribute to higher ratio of

Source of variation	SS ¹	DF ²	BB MS ³	F-value	p-value	SS	df	TB MS	F-value	P-value
Model	2641.7	20	132.09	29.3	< 0.0001	1032.5	20	51.624	23.896	< 0.0001
A	790.34	1	790.34	175.31	< 0.0001	0.006375	1	0.006375	0.002951	0.95705
B	152.4	1	152.4	33.806	< 0.0001	34.779	1	34.779	16.099	0.000387
C	173.86	1	173.86	38.565	< 0.0001	122.59	1	122.59	56.744	< 0.0001
D	274	1	274	60.78	< 0.0001	151.63	1	151.63	70.19	< 0.0001
E	142.82	1	142.82	31.681	< 0.0001	237.04	1	237.04	109.72	< 0.0001
AB	130	1	130	28.837	< 0.0001	2.349	1	2.349	1.0873	0.30568
AC	92.797	1	92.797	20.584	< 0.0001	237.04	1	237.04	109.72	< 0.0001
AE	3.1527	1	3.1527	0.69934	0.40984	40.892	1	40.892	18.928	0.00015329
AD	22.358	1	22.358	4.9594	0.033875	7.8379	1	7.8379	3.6281	0.066774
BC	47.031	1	47.031	10.432	0.0030738	17.844	1	17.844	8.2596	0.0075123
BE	8.2152	1	8.2152	1.8223	0.18748	4.1742	1	4.1742	1.9322	0.1751
BD	0.85908	1	0.85908	0.19056	0.66568	0.82382	1	0.82382	0.38133	0.54171
CD	42.42	1	42.42	9.4096	0.0046433	35.68	1	35.68	16.516	0.000336
CE	0.035643	1	0.035643	0.0079064	0.92976	0.27313	1	0.27313	0.12643	0.72474
DE	2.2820	1	2.2820	0.50619	0.48248	1.1024	1	1.1024	0.51027	0.48073
A ²	282.67	1	282.67	62.703	< 0.0001	4.2703	1	4.2703	1.9766	0.17037
B ²	4.5823	1	4.5823	1.0165	0.32170	101.15	1	101.15	46.823	< 0.0001
C ²	221.53	1	221.53	49.141	< 0.0001	155.33	1	155.33	71.9	< 0.0001
D ²	133.09	1	133.09	29.522	< 0.0001	21.232	1	21.232	9.8279	0.0039161
E ²	33.624	1	33.624	7.4586	0.010629	9.9045	1	9.9045	4.5846	0.040793
Residual	130.74	29	4.5081			62.651	29	2.1604		
Lack of Fit	108.51	20	5.4257	2.1974	0.11253	47.455	20	2.3728	1.4054	0.30761
Pure Error	22.222	9	2.4691			15.195	9	1.6884		
Cor Total	2772.5	49				1095.1	49			

dye molecules to the vacant sites of the adsorbent. Fig. (6d) sonication time it can be concluded that maximum adsorption of TB could be achieved when the sonication time was increased.

Optimization of CCD by DF for extraction procedure

The profile for desirable option with predicted values in the STATISTICA 10.0 software

was used for the optimization of the process (Fig.7). The desirability in the range of 0.0 (undesirable) to 1.0 (very desirable) was used to obtain a global function (D) that is the base of optimization. The CCD design matrix results were obtained as maximum (100 % and 100%) and minimum (67.99% and 67.99%) for BB and TB, respectively. According to these values, DF settings for either of dependent variables of removal percentages were depicted on

Table 4: Various isotherm constants and their correlation coefficients calculated for the adsorption of BB and TB on to Mn-Fe₂O₄-NPs-AC

Isotherm	Equation	parameters	Value of parameters for BB	Value of parameters for TB
Langmuir	$q_e = q_m b C_e / (1 + b C_e)$	Q_m (mg g ⁻¹)	70.3	48.48
		K_a (L mg ⁻¹)	10.49	1.344
		R^2	0.99	0.97
Freundlich	$\ln = \ln K_F + (1/n) \ln C_e$	1/n	3.81	3.96
		K_F (L mg ⁻¹)	9.44	4.67
		R^2	96	0.93
Tempkin	$q_e = B_1 \ln K_T + B_1 \ln C_e$	B_1	15.55	10.63
		K_T (L mg ⁻¹)	106.75	9.3
		R^2	0.98	0.94
Dubinin-Radushkevich (DR)	$\ln q_e = \ln Q_s - B \hat{a}^2$	Q_s (mg g ⁻¹)	60.35	29.135
		B	6E-07	5E-07
		E (kJ mol ⁻¹)	8535.53	3354.1
		R^2	0.97	0.93

Table 5: Various Kinetic constants and their correlation coefficients calculated for the adsorption of BB and TB onto Mn-Fe₂O₄-NPs-AC

Model	parameters	Value of parameters for BB	Value of parameters for TB
pseudo-First-orderkinetic	k_1 (min-1)	1.43	0.987
	q_e (calc) (mg g-1)	10.155	17.92
	R^2	0.95	0.95
pseudo-Second-order kinetic	k_2 (min-1)	0.507	0.154
	q_e (calc) (mg g ⁻¹)	53.46	56.15
	R^2	0.999	0.999
Intraparticlediffusion	K_{diff} (mg g-1 min-1/2)	4.59	8.05
	C (mg g ⁻¹)	40.71	33.77
	R^2	0.94	0.97
Elovich	β (g mg-1)	1.379	0.609
	α (mg g-1 min-1)	22596	17074
	R^2	0.94	0.98
q_e (exp) (mg g ⁻¹)		51.45	52

Table 6: Thermodynamic parameters for the adsorption of BB and TB onto Mn-Fe₂O₄-NPs-AC

Parameter	Temperature (K)	BB		TB		
		308.15	318.15	308.15	318.15	
ΔG°	288.15	308.15	318.15	308.15	318.15	338.15
	-9257.46	-10376	-12082.3	-11697.6	-14274.7	-20213
Kc	47.66	57.4	96.33	132	220.66	1329
ΔH° kj mol ⁻¹	29.238			165.25		
ΔS° j mol ⁻¹ k ⁻¹	131.4859			32.488		
				150.55		

the right hand side of Fig.7. Desirability of 1.0 was assigned for maximum removal (100% and 100%), 0.0 for minimum (67.99% and 67.99%) and 0.5 for middle (83.995 and 83.995 %) for BB and TB, respectively. The individual desirability scores are illustrated on the left hand side of Fig.7 (bottom). The overall response obtained from these plots was depicted at the top (left) of Fig.7. Based on these calculations and desirability score of 1.0, maximum recoveries (100 % and 100%) for BB and TB, respectively were obtained at optimum conditions as: 5 min for sonication time, 0.03g for adsorbent mass, 12 mg/L for BB and 12 mg/L for TB at pH 6. Five solutions with different amounts of ideal conditions were used to predict the optimum conditions for BB and TB dyes adsorption on to Mn-Fe₂O₄- NPs-AC. The validity of the predicated responses at the optimized conditions was checked by performing duplicate experiments at similar conditions with RSD lower than 2% and removal percentage more than 98.5% in good agreement with the predicted value. This strong agreement proves that the predictive model found based on RSM is well applicable for describing the removal percentages of dyes studied against the variables involved.

Adsorption equilibrium study

Adsorption equilibrium isotherm is designed based on mathematical relation of the amount of adsorbed target per gram of adsorbent ((mg/g)) to the equilibrium non-adsorbed amount of dye in solution (C_e (mg/L) at fixed temperature^{30,31}. Isotherm studies are divided to well-known models such as Langmuir, Freundlich, Temkin and Dubinin–Radushkevich based on well-known conditions. The Langmuir model is the most frequently employed model given by following equation³²:

$$q_e = \frac{Q_m K_L C_e}{1 + K_L C_e} \quad \dots(7)$$

Where and K_L are the concentration of adsorbate at equilibrium (mg/L), maximum monolayer adsorption capacity(mg/g) and Langmuir constant(L/mg), respectively. was plotted against where parameters such as , K_L , and R^2 were calculated based on the slope and intercept of such lines and displayed in Table4. The values of K_a (the Langmuir adsorption constant (L/mg)) and Q_m (theoretical maximum adsorption capacity (mg/g))

Table 7: Comparison for the removal of BB by different methods and adsorbents

Adsorbent	Contact time(min)	Sorption capacity (mg g ⁻¹)	References
Magnetically modified spent coffee grounds	90	69.2	[42]
Magnetic fluid modified peanut husks	90	95.3	[43]
Modified Form Iron OxideNanosphere	1440	54.9	[44]
Iron OxideNanosphere	1440	33.8	[44]
Mn-Fe ₂ O ₄ - NPs-AC	5	70.3	This work

were obtained from the intercept and slope of the plot of *versus* C_e , respectively. The applicability of Langmuir model for the interpretation of the experimental data over the whole concentration range is proven from high correlation coefficient at all adsorbent masses. The increase in the amount of adsorbent leads to significant enhancement in the actual amount of adsorbed dye. The parameters of Freundlich isotherm model such as K_F and the capacity of the adsorption were calculated from the intercept and slope of the linear plot of \ln *versus* \ln , respectively. The heat of the adsorption and the adsorbent–adsorbate interaction were evaluated by using Temkin isotherm model. In this model, B is the Temkin constant related to heat of the adsorption (J/mol), T is the absolute temperature(K), R is the universal gas constant(8.314J/mol. K) and K is the equilibrium binding constant(L/mg). D–R model was applied to estimate the porosity apparent free energy and the characteristic of adsorption^{33,34}. In this model B (mol²/k) is a constant related to the adsorption energy, Q_s (mg/g) is the theoretical saturation capacity and E is the Polanyi potential. The slope of the plot of \ln *versus* E^2 gives B and its intercept yields the value. The linear fit between the plot of \ln *versus* and calculated correlation coefficient (R^2) for Langmuir isotherm model shows that the dye removal isotherm can be better represented by Langmuir model (Table4). This confirms that the adsorption of dyes takes place at specific homogeneous sites as a monolayer on to the Mn-Fe₂O₄- NPs-AC surface.

Kinetic study

Adsorption of a solute by a solid in aqueous solution through complex stages³⁵ is strongly influenced by several parameters related to the

state of the solid (generally with very heterogeneous reactive surface) and to physico-chemical conditions under which the adsorption occurred. The rate of dyes adsorption onto adsorbent was fitted to traditional models like, pseudo-first, second-order, intraparticle and Elovich models. The Lagergren pseudo-first order modeled described the adsorption kinetic data³⁶. The Lagergren is commonly expressed as follows:

$$\frac{dq_t}{dt} = k_1 (q_e - q_t) \quad \dots(8)$$

Where q_e and q_t are the adsorption capacities at equilibrium and at time t , respectively. k_1 is the rate constant of the pseudo-first-order adsorption(L/min). The $\log(q_e - q_t)$ *versus* t was plotted and the values of k_1 and q_e were determined by using the slope and intercept of the line, respectively.

$$\log (q_e - q_t) = \log q_e - \left(\frac{k_1}{2.303} \right) t \quad \dots(9)$$

The fact that the intercept is not equal to $\log q_e$ imply that there action is unlikely to follow the first-order³⁷. The relationship between initial solute concentration and rate of adsorption is linear when pore diffusion limits the adsorption process. Therefore, it is necessary to fit experimental data to another model (Table5) such as pseudo-second order model³⁸, based on the following equation:

$$\frac{dq_t}{dt} = k_2 (q_e - q_t)^2 \quad \dots(10)$$

Eq.(10) is integrated over the interval 0 to t for t and 0 to q_e for q_t to give

$$\frac{t}{q_t} = \frac{1}{k_2 q_e^2} + \frac{t}{q_e} \quad \dots(11)$$

As mentioned above, the plot of $\log(q)$ versus t does not show good results for entire sorption period, while the plot of t/q versus t shows a straight line. The values of k_2 and equilibrium adsorption capacity (q_e) were calculated from the intercept and slope of the plot of t/q versus t (Table5). The calculated q_e values at different working conditions like various initial dyes concentrations and/or adsorbent masses were close to the experimental data and higher R^2 values corresponding to this model confirm its more suitability for the explanation of experimental data. This indicates that the pseudo-second-order kinetic model applies better for the adsorption of BB and TB system for the entire sorption period the intraparticle diffusion equation is given as³⁹:

$$q_t = k_{dif} t^{1/2} + C \quad \dots(12)$$

Where k_{dif} is the intraparticle diffusion rate constant ($\text{mg}/(\text{g} \cdot \text{min}^{1/2})$) and C shows the boundary layer thickness. The linear form of Elovich model is generally expressed as⁴⁰:

$$q_t = \frac{1}{\beta} \ln(\alpha\beta) + \frac{1}{\beta} \ln t \quad \dots(13)$$

The kinetic data from pseudo-first and pseudo-second-order adsorption kinetic models as well as the intraparticle diffusion and Elovich model are given in Table5. The linear plots of $\ln(q)$ versus t indicated a good agreement between the experimental and calculated values for different initial dyes concentrations. Furthermore, the correlation coefficients of the pseudo-second-order kinetic model ($= 0.99$,) were greater than that of the pseudo-first-order model ($= 0.950$,). As a result, the adsorption fits to the pseudo-second-order better than the pseudo-first-order kinetic model.

Thermodynamic studies

The thermodynamic parameters, the values of enthalpy (ΔH^0), and entropy (ΔS^0), and Gibbs free

energy (ΔG^0), of the sorption are useful in defining whether the sorption reaction is endothermic or exothermic, and spontaneity of the adsorption process [40]. The adsorption standard free energy changes (ΔG^0) can be calculated according to:

$$\Delta G^0 = -RT \ln K_0 \quad \dots(14)$$

where R ($8.314 \text{ Jmol}^{-1} \text{ K}^{-1}$) is the ideal gas constant, and T (K) is the temperature. The negative ΔG^0 values at different temperatures were due to the fact that the adsorption process is spontaneous. The value of ΔG^0 decreased with an increase in temperature, indicated that the spontaneous nature of the adsorption of BB and TB dyes is inversely proportional to the temperature. The values of other parameters such as enthalpy change and entropy change may be determined from Van't Hoff equation:

The Thermodynamic parameters are listed in table 6. A positive standard enthalpy change suggests that the interaction of BB and TB by Mn- Fe_2O_4 - NPs-AC is endothermic, which supported by the increasing feasibility adsorption BB and TB with the increase in temperature towards Mn- Fe_2O_4 - NPs-AC.

Comparison of various adsorbent

The performance of the proposed method has been compared with other adsorbents (Table7). The adsorption capacity and contact time for our work are superior to other adsorbents to remove BB⁴¹⁻⁴⁴. The results indicated that the ultrasound-assisted removal method has a remarkable ability to improve the efficiency of dyes removal. The ultrasonic-assisted enhancement of dye removal could be attributed to the high-pressure shock wave and high speed microjets during the violent collapse of cavitation bubbles^{45,46}.

CONCLUSION

It is observed from the present study that the manganese ferrite nanoparticles loaded on activated carbon under the sonication is an efficient, fast and sensitive adsorption method for the removal of BB and TB. The influences of experimental parameters on the dyes removal percentages were

investigated by experimental design methodology (RSM). The adsorption characteristic was examined with the variations of pH, sonication time, Mn-Fe₂O₄- NPs-AC dosage, initial BB concentration and initial TB concentration. The removal of BB and TB from aqueous solutions in short time (5 min) is feasible with high removal percentage at optimum pH(6) which is neutral and is an advantage for the adsorption process. The equilibrium data were best described by the Langmuir model. The process kinetics can be success fully fitted with pseudo-second order model Thermodynamic constants were evaluated using equilibrium constants changing with temperature. The negative values of ΔG^0 indicate the spontaneity and positive values of ΔH^0 showed the

endothermic nature of BB and TB sorption. The data and methodology presented in this paper might be useful for designing the adsorbent for the treatment of actual effluent. Furthermore, the results of this study encourage the researches and industries to use ultrasound devices for more efficient dye adsorption. The optimized method was successfully applied to real wastewater samples.

ACKNOWLEDGEMENT

The author expresses their appreciation to the Science and Research Branch Islamic Azad University, Tehran, Iran for financial support of this work.

REFERENCES

- Robinson, T., McMullan, G., Marchant, R., and Nigam, P. (2001) *Bioresour. Technol.*, 77: 247–255.
- Slokar, Y.M. and Le Marechal, A.M. (1998) *Dyes Pigment*, 37: 335–356.
- Hao, J.O., Kim, H., and Chiang, P.C. (2000) *Crit. Rev. Environ. Sci Technol.*, 30: 449–505.
- Purkait, M.K., Das Gupta, S., and De, S. (2006) *J. Hazard. Mater.*, 136: 972–977.
- Purkait, M.K., Das Gupta, S., and De, S. (2004) *Sep. Purif. Technol.*, 37: 81–92.
- Hejazifar, M. and Azizian, S. (2012) *J. Dispersion Sci. Technol.*, 33: 846–853.
- Azizian, S., Haerifar, M., and Bashiri, H. (2009) *Chem. Eng. J.*, 146: 36–41.
- Yahyaee, B. and Azizian, S. (2012) *Chem. Eng. J.*, 209: 589–596.
- R.D.Lillie Ed. *Conns Biological Stains* 9th ed., Baltimore, MD, (1977), 145
- F. HUSSEIN, A. ALKHATEEB, and J. K. ISMAIL, CODEN ECJHAO *E-Journal of Chemistry*, Vol. 5, No. 2, pp ,(2008), 243-250
- S. Chikazumi, S. Taketomi, M. Ukita, M. Mizukami, H. Miyajima, M. Setogawa, Y. Kurihara, J. Magn. Mater. 65 (1987) 245.
- A. H. Lu, W. Schmidt, N. Matoussevitch, H. Bpnnermann, B. Spliethoff, B. Tesche, E. Bill, W. Kiefer, F. SchVth, *Angew. Chem.* 116 (2004) 4403.
- S. C. Tsang, V. Caps, I. Paraskevas, D. Chadwick, D. Thompsett. *Angew. Chem.* 116 (2004) 5763.
- A. K. Gupta, M. Gupta, *Biomaterials* 26 (2005) 3995.
- S. Mornet, S. Vasseur, F. Grasset, P. Verveka, G. Goglio, A. Demourgues, J. Portier, E. Pollert, E. Duguet, *Prog. Solid State Chem.* 34 (2006) 237.
- Z. Li, L. Wei, M. Y. Gao, H. Lei, *Adv. Mater.* 17 (2005) 1001.
- T. Hyeon, *Chem. Commun.* (2003) 927.
- D. W. Elliott, W. X. Zhang, *Environ. Sci. Technol.* 35 (2001) 4922.
- M. Takafuji, S. Ide, H. Ihara, Z. Xu, *Chem. Mater.* 16 (2004) 1977.
- S. Shahrokhian, S. Rastgar, M. K. Amini, M. Adeli, *Biochem*, 86 (2012) 78.
- Elibol M. *Process Biochem* 2002;38:667–73.
- Pavlovic MD, BunticAV, MihajlovskiKR, Siler-JTaiwanInst *Chem Eng* 2014; 45:1691–9.
- Hajati S, Ghaedi M, Yaghoubi S. mions and malachite green: Optimization by surface response methodology. *J Ind Eng Chem* 2015; 21:760–7.
- Hameed B, TanI, Ahmad A. Optimization of basic dye removal by oil palm fibre-based activated carbon using response surface methodology. *J Hazard Mater* 2008;158:324–

- 32.
25. Sahu J, Acharya J, Meikap B. Response surface modeling and optimization of chromium (VI) removal from aqueous solution using Tamarind wood activated carbon in batch process. *J Hazard Mater* 2009;172:818–25.
26. Myers RH, Montgomery DC, Anderson-Cook CM. *Response surface methodology: process and product optimization using designed experiments*. John Wiley & Sons; 2009.
27. Alenović CA, Dotsikas Y, Mašković CM, Janjić I, C-Stojanović CB, Ivanović CD, Medenica M. Desirability-based optimization and its sensitivity analysis for the perindopril and its impurities analysis in a microemulsion LC system. *Microchem J* 2011; 99: 454–60.
28. Roosta M, Ghaedi M, Daneshfar A, Darafarin S, Sahraei R, Purkait M. Simultaneous ultrasound-assisted removal of sunset yellow and erythrosine by Zn S: Nanoparticles loaded on activated carbon: optimization by central composite design. *Ultrason Sonochem* 2014;21:1441–50.
29. R. D. Waldron, *Phys. Rev.* 99 (1955) 1727.
30. Asfaram A, Ghaedi M, Agarwal S, Tyagi, Kumar Gupta V. Removal of basic dye Auramine-O by Zn S: Nanoparticles loaded on activated carbon: optimization of parameters using response surface methodology with central composite design. *RSC Adv* 2015;5:18438–50.
31. HoY-S, McKay G. The kinetics of sorption of divalent metal ions on sphagnum moss peat. *Water Res* 2000;34:735–42.
32. Langmuir I. The constitution and fundamental properties of solids and liquids. Part I. Solids. *J Am Chem Soc* 1916; 38:2221–95.
33. Radushkevich L. Potential theory of sorption and structure of carbons. *J Phys Chem* 1949; 23: 1410–20.
34. Culzoni MJ, Schenone AV, Llamas NE, Garrido M, DiNezio MS, Fernández B and BS, et al. Fast chromatographic method for the determination of dyes in beverages by using high performance liquid chromatography—diode array detection data and second order algorithms. *J Chromatogr A* 2009; 1216:7063–70.
35. HoY-S. Second-order kinetic model for the sorption of cadmium on tree fern: a comparison of linear and non-linear methods. *Water Res* 2006; 40:119–25.
36. Juang R, Wu F, Tseng R. The ability of activated clay for the adsorption of dyes from aqueous solutions. *Environ Technol* 1997;18:525–31.
37. Robinson T, McMullan G, Marchant R, Nigam P. Remediation of dyes in textile effluent: a critical review on current treatment technologies with a proposed alternative. *Bioresour Technol* 2001;77:247–55.
38. Wood GO. Review and comparison of D/R models of equilibrium adsorption of binary mixtures of organic vapors on activated carbons. *Carbon* 2002;40:231–9.
39. Weber W, Morris J. Kinetics of adsorption on carbon from solution. *J Sanit Eng Div Am Soc Civ Eng* 1963; 89:31–60.
40. HoY-S, McKay G. Pseudo-second order model for sorption processes. *Process Biochem* 1999; 34: 451–65.
41. C. Namasivayam, R.T. Yamuna, Adsorption of chromium by a low-cost adsorbent: biogas residual slurry, *Chemosphere* 30 (1995) 561–578.
42. Ivo Safarik, Katerina Horska, Barbora Svobodova, Mirka Safarikova. (2012). Magnetically modified spent coffee grounds for dyes removal. *Eur Food Res Technol.*, 234, 345-350.
43. Ivo Safarik, Mirka Safarikova. (2010). Magnetic fluid modified peanut husks as an adsorbent for organic dyes removal. *Physics Procedia.*, 9, 274-278.
44. Maryam Khosravi, Bahareh Yahyaei, and Saeid Azizian, Adsorption of Bismarck Brown by Iron Oxide Nanosphere and Its Modified Form, *Journal of Dispersion Science and Technology*, 35 (2014): 1135–1142,
45. Shirsath S, Pinjari D, Gogate P, Sonawane S, Pandit A. Ultrasound assisted synthesis of doped TiO₂ nanoparticles: characterization and comparison of effectiveness for photocatalytic oxidation of dye stuff effluent. *Ultrason Sonochem* 2013; 20: 277–86.
46. Gogate PR, Sutkar VS, Pandit AB. Sonochemical reactors: important design and scale up considerations with a special emphasis on heterogeneous systems. *Chem Eng J* 2011; 166:1066–82.